RESEARCH ARTICLE SUMMARY

NEURODEVELOPMENT

Stellate cells drive maturation of the entorhinal-hippocampal circuit

Flavio Donato,* R. Irene Jacobsen, May-Britt Moser, Edvard I. Moser*

INTRODUCTION: Maturation of cortical circuits depends on postnatal excitatory activity that spreads in a bottom-up manner from the sensory organs. Such activity is necessary for the formation and stabilization of computationally efficient synaptic networks. Whether similar activity is required to set up connectivity across the entire cortex, beyond the sensory regions, remains to be determined. In one high-end associative network involving the entorhinal cortex and hippocampus, the spatially tuned firing of place, grid, border, and head direction cells emerges during a protracted period of postnatal life. The appearance of a functional map of self-location in this system may reflect local computations enabled by the gradual maturation of local network topology.

RATIONALE: If spatial tuning arises as a consequence of specific network topology, then the emergence of functionally specific cell types during development should coincide with network maturation. We investigated microcircuit development during the second to fourth postnatal week in mice when the network of functionally specific cells in the medial entorhinal cortex takes on adult-like firing properties. Network-wide changes in the expression of maturation-related molecular markers (doublecortin, parvalbumin, and bassoon-positive synaptic puncta) were measured across multiple areas to reveal the temporal profile of maturation across subfields of the entorhinal-hippocampal circuit. To determine how circuit development is influenced by excitatory activity across subfields of the network, we used a targeted pharmacogenetic approach by which cells in different regions, with different projection patterns or different birth dates, could be silenced selectively during defined time windows.

RESULTS: Maturation of the hippocampal-entorhinal network followed a stereotyped sequence, where layer 2 of the medial entorhinal cortex (MEC-L2) was the first area to mature, followed by (in chronological order) CA3, CA1, dentate gyrus (DG), subiculum (SUB), layer 5 of the medial and lateral entorhinal cortex (MEC-L5 and LEC-L5, respectively), and, finally, layer 2 of the lateral entorhinal cortex (LEC-L2). At each stage of the circuit, excitatory activity was necessary for the maturation of downstream areas of the network, pointing to a linear and directional developmental sequence. This sequence originated in MEC-L2, where maturation of stellate cells preceded that of any other excitatory cell type in the circuit. Cell type–specific pharmacogenetic silencing revealed that activity in MEC-L2 stellate cells was necessary for maturation of the rest of the entorhinal-hippocampal network. Maturation of stellate cells themselves was independent of local excitatory activity but depended instead on when the stellate cells were born. Silencing layer 2 pyramidal cells had no effect on circuit maturation. The stellate cell–dependent arrest of maturation was more efficient if the silenced cells were born on the same day, suggesting that isochronic cohorts of stellate cells act synergistically to drive network maturation.

ON OUR WEBSITE

Read the full article at http://dx.doi.org/10.1126/science.aai8178

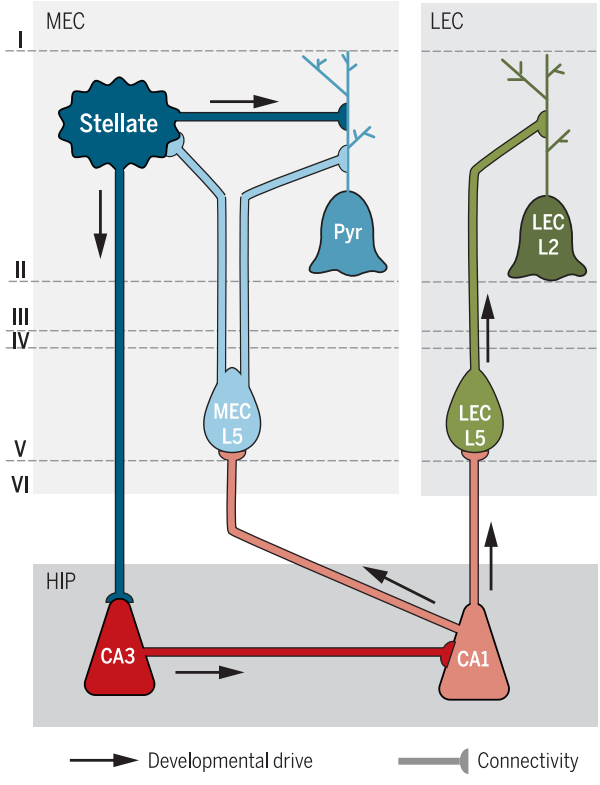

Superficial layers of the entorhinal cortex have both direct and indirect projections to hippocampal subfields. Indirect projections form a unidirectional loop—the trisynaptic pathway—through the hippocampus. Direct projections reach each subfield. CA1 pyramidal cells in the hippocampus establish connections back to the deep layers of the entorhinal cortex, from where information is relayed up to layer 2 (gray lines). During development, excitatory activity originating from MEC-L2 instructs maturation of the entorhinal-hippocampal circuit in a linear sequence recapitulating excitatory information flow through the adult network (black arrows). Stellate cells are at the top of the developmental hierarchy: Silencing stellate cells, but not pyramidal neurons, is sufficient to arrest the progression of maturation across the remaining entorhinal-hippocampal circuit.

CONCLUSION: Our data show that the entorhinal-hippocampal circuit matures in a linear sequence that begins with stellate cells in MEC-L2 and propagates sequentially through the subfields of the transverse entorhinal-hippocampal circuit, recapitulating the flow of excitation through the circuit in adult animals. Maturation of stellate cells themselves may be determined intrinsically in a neurogenesis-dependent manner. The dependence on neurogenesis may parcel the stellate network into cohorts of isochronic neurons that act synergistically during development and give rise to independent subnetworks in the circuit. We propose that, during development, stellate cells are the source of an activity-dependent instructive signal that drives maturation of the entorhinal-hippocampal network underlying spatial representation in the brain. A small number of autonomously developing neuronal populations, similar to entorhinal stellate cells, may function as intrinsic drivers of maturation in different regions of the cortex. ■

Kavli Institute for Systems Neuroscience and Centre for Neural Computation, Norwegian University of Science and Technology, Olav Kyrres gate 9, Norwegian Brain Centre, 7491 Trondheim, Norway.
*Corresponding author. Email: flavio.donato@ntnu.no (F.D.); edvard.moser@ntnu.no (E.I.M.)
Cite this article as F. Donato *et al.*, *Science* 355, eaai8178 (2017). DOI: 10.1126/science.aai8178

RESEARCH ARTICLE

NEURODEVELOPMENT

Stellate cells drive maturation of the entorhinal-hippocampal circuit

Flavio Donato,* R. Irene Jacobsen, May-Britt Moser, Edvard I. Moser*

The neural representation of space relies on a network of entorhinal-hippocampal cell types with firing patterns tuned to different abstract features of the environment. To determine how this network is set up during early postnatal development, we monitored markers of structural maturation in developing mice, both in naïve animals and after temporally restricted pharmacogenetic silencing of specific cell populations. We found that entorhinal stellate cells provide an activity-dependent instructive signal that drives maturation sequentially and unidirectionally through the intrinsic circuits of the entorhinal-hippocampal network. The findings raise the possibility that a small number of autonomously developing neuronal populations operate as intrinsic drivers of maturation across widespread regions of the cortex.

To create a neural representation of the external world, sensory stimuli are topographically mapped onto highly organized neural networks spanning multiple sensory areas in the neocortex (*1*–*4*). The early development of such topographical sensory representations depends strongly on spontaneous and sensory-driven neural activity spreading bottom-up from sensory receptors to sensory cortices (*5*–*8*).

Like in the sensory systems, the brain's representation of space relies on an extended network of specialized cell types spanning multiple interconnected brain regions. Cell types involved in the representation of space include place cells in the hippocampus and grid, border, head direction, and speed cells in the medial entorhinal cortex (MEC) (*9*). Properties of these cells are thought to reflect the intrinsic connectivity of the MEC (*10*) as well as the unique unidirectional organization of entorhinal projections through the hippocampus (fig. S1A) (*11*–*14*). However, in contrast to the primary sensory cortices, little is known about how the entorhinal-hippocampal microcircuit is assembled during development, or what role neural activity has in refining the connectivity and maturation of the circuit. Place, border, and head direction cells exhibit adult-like features from the onset of spatial navigation at 2 to 3 weeks of age (*15*–*18*), whereas the periodic firing pattern of grid cells emerges later at about 4 weeks of age (*15*, *16*). The spatial accuracy of place cells evolves with a similarly protracted time course (*15*, *16*, *19*), suggesting that early interactions between subregions of the network might be crucial for the eventual emergence of spatially specific firing.

With these parallels in mind, we sought to determine how structural elements of the entorhinal-hippocampal circuit are wired together during development. We monitored network-wide developmental changes in the expression of maturation-related anatomical markers, taking advantage of targeted pharmacogenetic silencing methods to determine whether activity in any elements of the circuit had particular functions in organizing maturation across the network as a whole. Our data show that the entorhinal-hippocampal circuit matures in a linear sequence that recapitulates excitatory information flow through the adult hippocampal network. Excitatory activity at each stage of the circuit was necessary for the development of the following stages. Stellate cells in MEC-L2 were at the top of this developmental hierarchy, providing an instructive signal that drove maturation across the entire entorhinal-hippocampal network.

Kavli Institute for Systems Neuroscience and Centre for Neural Computation, Norwegian University of Science and Technology, Olav Kyrres gate 9, Norwegian Brain Centre, 7491 Trondheim, Norway. ***Corresponding author. Email: flavio.donato@ntnu.no (F.D.); edvard.moser@ntnu.no (E.I.M.)**

Stagewise maturation of the transverse hippocampal circuit

To determine the temporal profile of maturation among identified populations of neurons in the entorhinal-hippocampal network, we first monitored the expression of doublecortin (DCX) in each area of the network during the first postnatal month. DCX is a microtubule-associated protein that is present in neuronal precursors and immature neurons, where it promotes dendritic growth and is down-regulated during the stabilization of synaptic connectivity at late developmental stages (*20*, *21*). In adults, the protein is expressed only in immature neurons in areas with ongoing neurogenesis (*21*). Because of this unique association with immature neurons, we used DCX as a marker of the maturational state of different classes of entorhinal and hippocampal neurons. For each region or cell class, we quantified for every third day the fraction of neurons in which DCX expression had declined to undetectable levels (Fig. 1A and fig. S1). We subsequently identified for each region or cell type the first day on which this fraction constituted 80% or more of the $NeuN^+$ cells (Fig. 1C). The quantification was validated by testing it on entorhinal-hippocampal sections from adult mice (P90 to P120). As expected, there were virtually no DCX^+ neurons in any of the areas analyzed, in line with published values (*21*), except for the DG, where adult neurogenesis accounts for DCX expression in progenitors and immature neurons [fraction of DCX^+ cells: 0.05 ± 0.01, as in (*22*)] (Fig. 1B).

DCX was expressed extensively in all entorhinal-hippocampal areas at P5 but subsequently declined (fig. S1). Analysis of DCX levels revealed that the maturation was staggered between subregions of the circuit (Fig. 1C). Stellate cells in layer 2 of the medial entorhinal cortex (MEC-L2 St) were the first to mature (80% threshold crossed at P14), followed (in chronological order) by pyramidal cells in MEC layer 2 (MEC-L2 Pyr) and CA3 (P20), CA1 (P23), dentate gyrus (DG), subiculum (SUB), layer 5 of the medial (MEC-L5) and lateral (LEC-L5) entorhinal cortices (all P26), and, finally, layer 2 of the lateral entorhinal cortex (LEC-L2; >P30). Hierarchical clustering of the maturation curves for these areas identified synchronous maturation profiles for cell populations with similar synaptic distances from the stellate cells (Fig. 1D), suggesting that maturation occurred in successive waves through the intrinsic hippocampal circuit, with MEC-to-hippocampal directionality.

To support the DCX-based observations with an independent measure, we analyzed the time course of maturation in an inhibitory cell type. In fast-spiking interneurons, cytosolic expression of the protein parvalbumin (PV) has been correlated with their structural and functional maturation, as well as synaptic integration in the circuit (*23*). Thus, we conducted a confocal-based analysis of PV expression in single neurons in each area of the entorhinal-hippocampal network (see fig. S1D and Supplementary Materials and Methods). PV expression was staggered between regions in a sequence that mirrored the stepwise down-regulation of DCX. MEC-L2 was the first area to up-regulate PV expression (threshold set as in Fig. 1C and crossed by P17), followed by CA3 (P20), CA1, MEC-L5, SUB, and DG (all P26), LEC-L5 (P30), and LEC-L2 (>P30) (Fig. 1E and fig. S1D).

Finally, as a third independent marker of maturation in the entorhinal-hippocampal neural circuit, we investigated synaptogenesis by assessing the increase in density of synaptic puncta in the developing cortex. To estimate synaptic density, we performed immunological staining for the protein Bassoon (Bs), which localizes at the active zone of presynaptic nerve terminals (*24*). The local density of Bs puncta was normalized to the local density of puncta in the corresponding adult network (P90 to P120). Again, time courses were staggered between subregions and subpopulations in a sequence that matched the flow of information through the adult circuit. MEC-L2 was the first to demonstrate increased density of Bs puncta (threshold set as in Fig. 1C and crossed at P17), followed by CA3 (P20), CA1 (P23), DG, SUB, MEC-L5, and LEC-L5 (all P26), and finally LEC-L2 (>P30) (Fig. 1F).

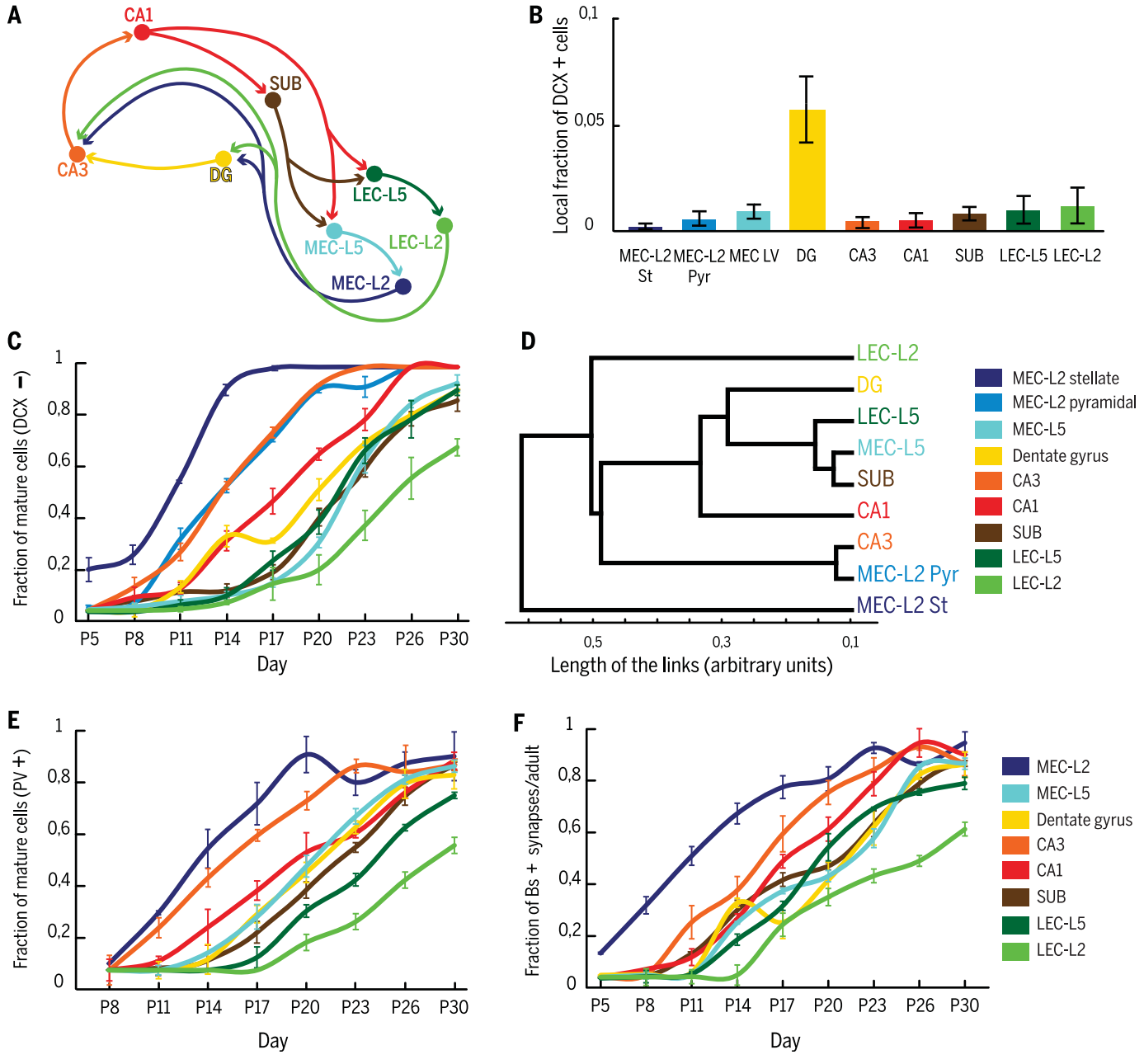

Fig. 1. Stagewise sequential maturation of the entorhinal-hippocampal network. (**A**) Schematic representation of information flow in the transverse entorhinal-hippocampal circuit (*49*–*53*). (**B**) Validation of DCX$^+$ quantification in adult mice (P90 to P120) (>1500 cells from three mice). (**C**) Fraction of neurons with DCX expression levels below the detection limit in each local network during successive days of maturation (DCX$^-$, cumulative distributions, means ± SD; >120,000 neurons from three mice for each time point). (**D**) Hierarchical clustering of data in (C); *x* axis: length of the links of the dendrogram, arbitrary units. MEC-L2 St is the first population to exhibit dissimilarity from the rest of the network, followed by (i) MEC-L2 Pyr and CA3, (ii) CA1, (iii) DG, SUB, MEC-L5, and LEC-L5, and (iv) LEC-L2. (**E**) Fraction of cells in each local network exhibiting PV expression (PV$^+$) at successive stages of maturation. Cumulative distributions are normalized to adult levels of PV$^+$ neurons in each local network (means ± SD, >45,000 neurons from three mice). (**F**) Density of synaptic puncta in each local neuropil volume normalized to adult levels for each area. Synaptic puncta are identified by the expression of the protein Bassoon (Bs$^+$). Adult levels are quantified at P90 as number of puncta/neuropil μm^3 (means ± SD, nine independent areas from three mice for each time point).

Together, the data suggest that maturation of the hippocampal-entorhinal network follows a stereotyped sequence that recapitulates the stagewise unidirectional flow of information through the intrinsic hippocampal microcircuit. DG provided the only exception to this scheme. The temporal profile of maturation in dentate granule cells was closer to that of cells in the deep layers of the entorhinal cortex than to downstream CA3 (Fig. 1D). This exceptional time profile is in line with the late peak of neurogenesis in DG, which extends through the first postnatal week (*25*, *26*).

Excitatory activity instructs stagewise circuit maturation

The sequential maturation of the entorhinal-hippocampal circuit raises the possibility that maturation is caused by an instructive signal that originates at the first step in the sequence, in

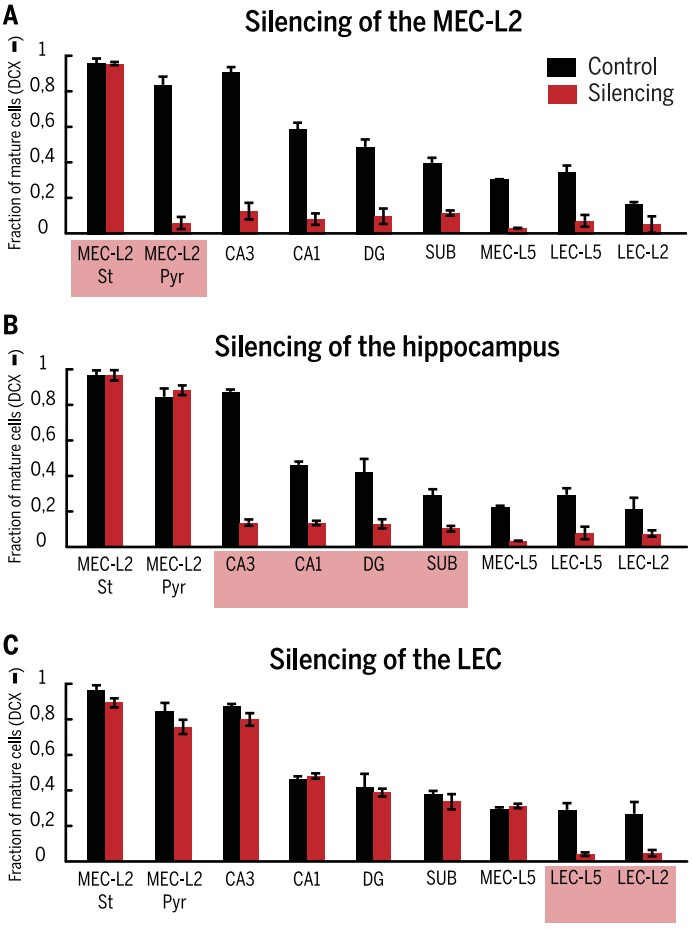

Fig. 2. Excitatory activity in MEC-L2 provides an instructive signal for maturation across stages of the entorhinal-hippocampal circuit. (**A**) Local fraction of DCX$^-$ neurons (means ± SD) in control animals (black bars) and CNO animals upon MEC-L2 silencing (red bars). *X* axis, region of the entorhinal-hippocampal network; *y* axis, fraction of NeuN$^+$ cells with DCX levels below the detection limit; >24,000 cells from at least three animals per group. Three categorically different classes of treatments were pooled to form the control group: (i) no virus, no CNO; (ii) virus, no CNO; and (iii) no virus, CNO. (**B**) DCX expression upon hippocampus-specific silencing [>24,000 cells from at least three animals per group; controls pooled across three categorically different classes of treatment, as in (A)]. (**C**) DCX expression upon LEC-specific silencing (>24,000 cells from at least three animals per group; controls pooled as above).

MEC-L2, and then propagates synaptically through the network over the course of many days. Such a signal could take the form of excitatory neural activity, which is known to shape the maturation of cortical columns in the sensory cortices (*4*). To determine whether activity is necessary for maturation also in the entorhinal-hippocampal network, we used inhibitory Designer Receptors Exclusively Activated by Designer Drugs (DREADDs) and silenced cell populations at different stages of the circuit for up to 6 days during early postnatal development [fig. S2A (*27*)]. A viral mix targeting hM4D(Gi) to excitatory neurons was injected in entorhinal or hippocampal subregions in newborn pups (P1). Infected neurons were silenced 2 weeks after injection, from P14 to P20, when hM4D expression was extensive (fig. S3, A to C). hM4D receptors were activated by continuous delivery of the ligand clozapine-*N*-oxide (CNO) (1 mg/kg) through an osmotic minipump implanted subcutaneously on the pups' backs. On the basis of the anatomical spread and specificity of the infection (>80% neurons infected in the target area and <20% cells infected in off-target areas; fig. S2, B and C), we focused on three groups of animals, with either MEC-L2–, hippocampus-, or LEC-specific DREADD expression. As expected, if activity were silenced, then CNO produced a decrease in the fraction of c-FOS$^+$ cells in all areas expressing the viral construct. In the silenced groups, c-FOS was also reduced in downstream regions of the circuit (fig. S3D).

The effect of silencing on circuit maturation was estimated at the end of the silencing window, on P20, by quantitative analysis of local DCX and PV expression as well as synaptic density. Silencing MEC-L2 prevented maturation across the whole entorhinal-hippocampal network. With the exception of the stellate cells of MEC-L2 itself, every cell population in the network exhibited significantly reduced levels of DCX$^-$ neurons at the end of the silencing window, when compared to nonsilenced control animals (means ± SD; Student's *t* test, t = 4.7 to 70.0 and $P < 0.0033$, except for stellate cells, t = 0.11 and P = 0.91; Fig. 2A and fig. S4A). In all areas, MEC-L2–specific silencing also prevented the maturation-related increase in PV expression ($t > 10.5$ and $P < 0.0001$; fig. S4B), as well as the increase in the density of synaptic puncta ($t > 8.5$ and $P < 0.0001$; fig. S4C). Together, these three lines of data suggest that excitatory activity from MEC-L2 is necessary for maturation of cell populations across the entire entorhinal-hippocampal network.

In contrast, maturation in MEC-L2 was not affected when activity was inhibited during the same interval in the hippocampus (t = 0.049 and P = 0.96 for stellate cells and t = 1.3 and P = 0.22 for pyramidal cells; Fig. 2B). However, after hippocampal inactivation, maturation was blocked in all areas within or downstream of the hippocampus (t = 7.4 to 68.5 and $P < 0.0003$; Fig. 2B). The retarded maturation of these areas was also expressed by the blocked increase of PV$^+$ neurons ($t > 10.1$ and $P < 0.0001$; fig. S4D) and densities of synaptic puncta ($t > 8.515$ and $P < 0.0001$; fig. S4E). PV$^+$ neurons and synaptic puncta were not altered in MEC-L2 (t = 0.18 and P = 0.10 and t = 0.20 and P = 0.80, respectively). These data suggest that excitatory activity from the hippocampus is necessary for the maturation of subfields within the hippocampus, as well as MEC-L5 and LEC, but dispensable for the maturation of the MEC-L2 circuit.

Finally, when inhibitory DREADDs were activated during the same time window in LEC, maturation was arrested only in LEC-L5 and LEC-L2, whereas no change in DCX could be observed in MEC or hippocampus ($t > 9.8$ and $P < 0.0001$ in LEC, but $t < 1.01$ and $P > 0.4$ elsewhere; Fig. 2C). The selective effect on maturation in LEC was confirmed by the failed increase of PV$^+$ neurons in LEC-L5 and LEC-L2 ($t > 5.1$ and $P < 0.0001$ in LEC, but $t < 0.95$ and $P > 0.2$ elsewhere; fig. S4F), as well as the absence of an increase in synaptic puncta in these two structures ($t > 8.1$ and $P < 0.0001$ in LEC, but $t < 1.5$ and $P > 0.52$ elsewhere; fig. S4G). These data imply that excitatory activity in LEC is necessary for maturation in LEC itself, but not for the rest of the entorhinal-hippocampal network.

Topography of MEC maturation

We next focused on the local circuit of the MEC. Quantification of DCX expression in deep and superficial MEC layers showed that maturation proceeds from dorsal to ventral in all layers. This developmental gradient confirms a previous observation (*28*) but extends it in the sense that DCX could here be monitored at single-cell resolution, with clear differentiation between stellate and pyramidal cells. Our analysis showed that, at every dorsoventral position, maturation of MEC-L2 stellate cells precedes that of pyramidal cells in layers 2 and 5 (Fig. 3, A and B, and fig. S5). The lag between stellate and layer 2 pyramidal cells was 3 to 6 days, whereas layer 5 neurons were delayed

by a further 3 to 6 days [two-way analysis of variance (ANOVA), neuronal subpopulation × Postnatal Day, including comparisons at every segment along the MEC: $F_{7,32} > 22.3$, $P < 0.0001$]. The progression of maturation from dorsal to ventral MEC was also observed in PV-expressing interneurons in superficial and deep layers (direct comparison between block I and more ventral segments: Group × Segment: $F_{7,32} > 14.2$, $P < 0.0001$; fig. S5).

To investigate whether the instructive signal that drives maturation through the transverse circuit is also responsible for maturation of the MEC, we silenced layer 2 cells in the MEC using inhibitory DREADDs in the same manner as in the transverse study. Silencing excitatory neurons in MEC-L2 did not change DCX levels in stellate cells at any dorsoventral level of the MEC [Group (silenced versus control): $F_{1,32} = 2.54$, $P = 0.81$; Group × Segment: $F_{7,32} = 0.42$, $P = 0.87$; Fig. 3C, left]. In contrast, the maturation-related

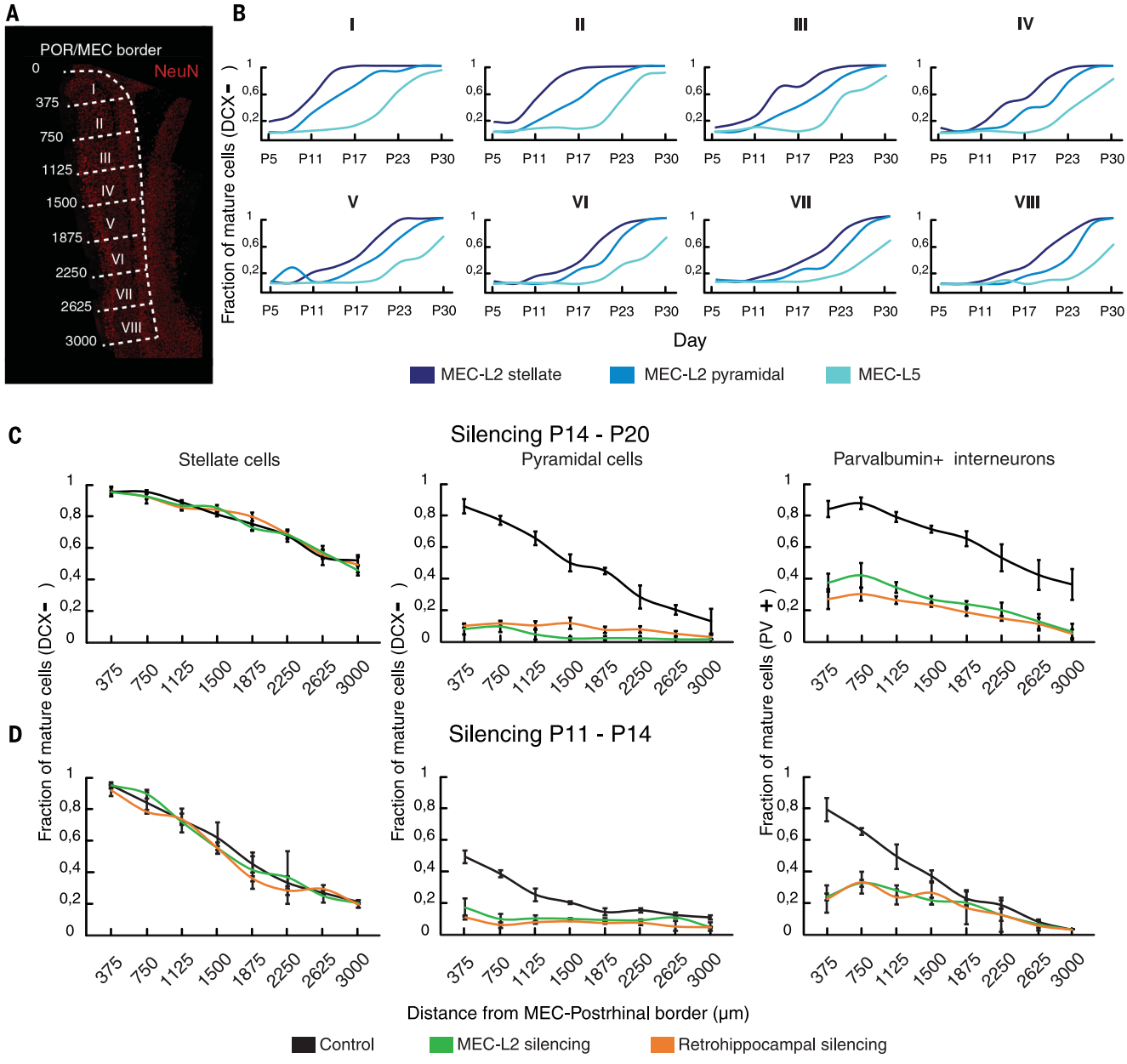

Fig. 3. Dorsoventral topographical maturation of MEC is driven by excitatory activity in L2. (**A**) The fraction of DCX$^-$ neurons was determined at eight positions of equal dimension (each 375 μm in length) along the dorsoventral axis of MEC (positions I to VIII) in a single sagittal section (NeuN$^+$ cells, red). Dorsal and ventral borders of MEC were identified as sharp transitions in L2 cell density [position 0 corresponding to the MEC-postrhinal cortex transition (MEC-POR); position 3000 corresponding to MEC-LEC transition]. The length of segment VIII was adjusted for early postnatal sections (P8 to P14) to account for change in brain size (therefore, the MEC-to-LEC transition always fell into this block). The total number of NeuN$^+$ cells in each block did not change significantly between P5 and P90 (except for block VIII). (**B**) Cumulative fractions of DCX$^-$ neurons in superficial and deep layers in every segment along the dorsoventral MEC axis. Stellate and pyramidal cells were distinguished on the basis of reelin and calbindin expression (>45,000 neurons from three animals per time point). (**C**) Fraction of DCX$^-$ excitatory neurons and PV$^+$ inhibitory neurons after silencing excitatory neurons selectively in MEC-L2 (green) or widely across retrohippocampal cortices (orange) between P14 and P20. Controls were pooled as in Fig. 2 (>210,000 neurons from at least three animals per treatment group). (**D**) Similar estimates of DCX and PV expression after silencing excitatory neurons in MEC-L2 (green) or retrohippocampal cortices (orange) between P11 and P14 (>60,000 neurons from at least three animals per treatment group).

increase in DCX$^-$ pyramidal cells was prevented along the entire dorsoventral MEC axis (MEC-L2 silencing in green, controls in black; two-way ANOVA, $F_{7,32} = 15.9$, $P < 0.0001$; Fig. 3C, middle). Silencing excitatory activity in MEC-L2 also affected PV expression in interneurons (Group × Segment: $F_{7,32} = 21.6$, $P < 0.0001$; Fig. 3C, right). The effect of inactivating MEC-L2 cells was dependent on the fraction of local excitatory cells infected (fig. S6A), regardless of their dorsoventral location. In all animals, the proportion of infected stellate and pyramidal cells was comparable to the overall proportion of these cell types in the network (fig. S2D).

In contrast to the rest of the MEC network, the maturation of stellate cells was not affected by silencing excitatory activity in any of the multiple regions they receive input from. We tested whether the maturation of stellate cells was affected when excitatory activity was silenced widely across areas of the ipsilateral retrohippocampal cortex that have projections to MEC-L2, such as postrhinal cortex and parasubiculum. Despite a significant disruption of maturation in pyramidal and PV neurons after silencing in these animals (Group: $F_{1,32} < 2.78$, $P > 0.082$; Group × Segment: $F_{7,32} > 7.42$, $P < 0.001$; Fig. 3C and fig. S6C, middle and right), there was still no effect on the fraction of DCX$^-$ stellate cells (Group: $F_{1,32} = 0.98$, $P = 0.93$; Group × Segment: $F_{7,32} = 2.30$, $P = 0.07$; Fig. 3C and fig. S6C, left), suggesting that stellate cells mature independently of activity in major afferent cell populations to MEC-L2. Further support for this conclusion comes from the observation that down-regulation of DCX expression in either stellate or pyramidal cells or up-regulation of PV expression in the interneuron population was unaffected when MEC was selectively deprived of homotopic contralateral inputs (fig. S6B).

We next asked whether the blockade of stellate cell maturation was ineffective because these cells or their inputs were silenced too late, given that the dorsal tip of MEC is already mature by P14. Silencing dorsal MEC-L2 or a larger portion of the ipsilateral retrohippocampal cortex between P11 and P14 before the network is mature (Fig. 1, C and E) did not produce any effect on the fraction of stellate cells expressing DCX at P14 (Fig. 3D, left). This result is corroborated by data from the ventral MEC. Although the ventral MEC network is still largely immature at P14 to P20, the maturation of stellate cells was not affected by silencing the MEC or upstream areas between P14 and P20 (Fig. 3C and fig. S6C). Together, these experiments rule out activity in MEC-L2 or afferent cell populations as an origin of the maturation signal for MEC-L2 stellate cells.

Finally, it is possible that the stagnation in DCX and PV levels after MEC-L2 silencing reflected not a delayed maturation but a functional impairment of pyramidal cells and interneurons. To address this possibility, we investigated whether the network was still able to progress through maturation if the brake induced by silencing was relieved. Specifically, we allowed a set of animals to recover from MEC inactivation by removing the osmotic minipump and thereby ending CNO delivery at P20 (fig. S7A). In these animals, after 6 days of recovery, the maturation of pyramidal cells and fast-spiking interneurons was indistinguishable from controls, that is, hM4D-expressing, saline-injected animals (DCX expression in fig. S7B: Group: $F_{1,32} = 2.84$, $P = 0.12$; Group × Segment: $F_{7,32} = 1.60$, $P = 0.10$; PV expression in fig. S7B: Group: $F_{1,32} = 1.26$, $P = 0.42$; Group × Segment: $F_{7,32} = 0.51$, $P = 0.43$). At an intermediate time point (P23; 3 days of recovery), DCX and PV expression levels were between those found in control animals and animals silenced without recovery (Group × Segment: $F_{7,32} > 7.2$, $P < 0.03$; fig. S7C). Surprisingly, in the recovering cohort of animals at P23, there was no dorsoventral topography in the maturation of pyramidal cells or PV$^+$ interneurons (flat curves in fig. S7D; slope of the linear regression along MEC is near 0; Student's t test, $t > 6.12$, and $P < 0.001$ when compared to age-matched controls; fig. S7E), suggesting that the activity signal that is necessary for driving maturation sequentially through the transverse entorhinal-hippocampal circuit may also participate in setting up the dorsoventral topography of pyramidal cells and PV$^+$ interneurons in MEC-L2. As expected, stellate cells

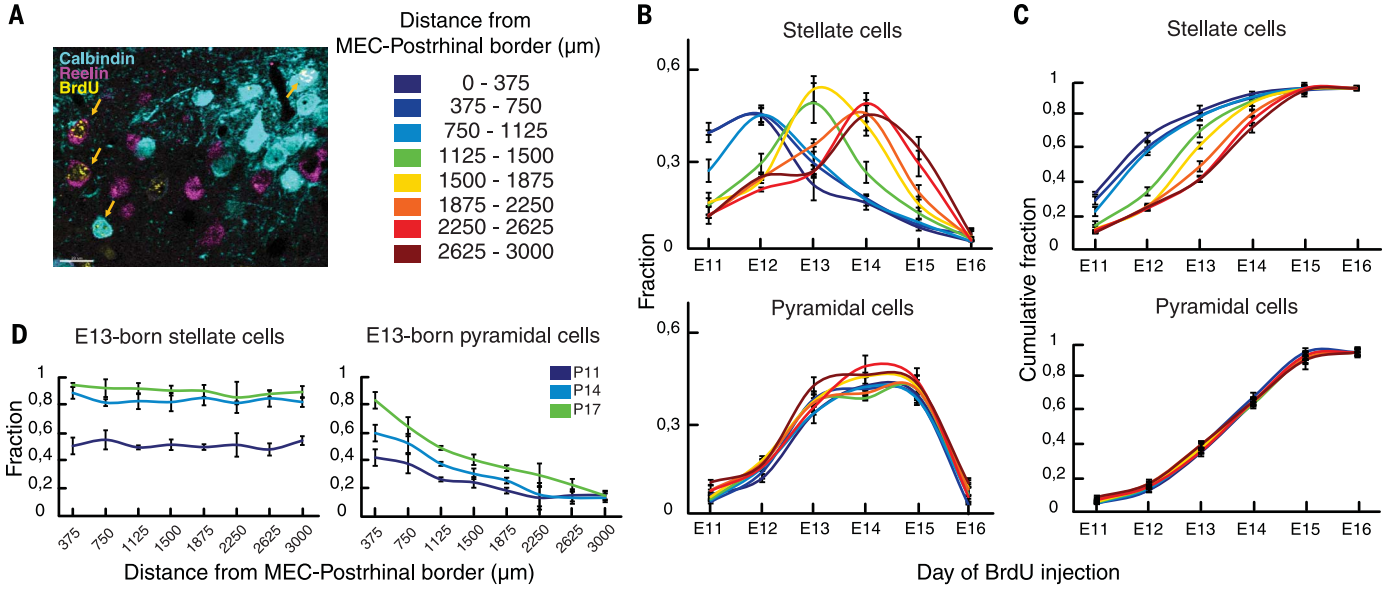

Fig. 4. Topographic distribution of stellate cells reflects progression of neurogenesis. (**A**) Expression of BrdU (yellow) in the adult MEC-L2 network as a result of BrdU injection in the pregnant mother (40× single confocal plane image from a sagittal section 3.5 mm lateral to the midline; reelin in magenta and calbindin in cyan; yellow arrows indicate stellate and pyramidal cells that are positive for BrdU). Anatomical mapping of isochronic cohorts of cells was performed at eight positions from the MEC-POR border (see Fig. 3A). Dorsoventral segments are color-coded. (**B**) Fraction of BrdU$^+$ stellate cells (top) and pyramidal cells (bottom) across embryonic days and segments along the dorsoventral MEC axis. In each segment, we counted the number of neurons positive for either reelin (Rl$^+$; stellate cells) or calbindin (Cb$^+$; pyramidal cells) and analyzed the proportions of these that stained for BrdU in the nucleus (means ± SD; >450,000 neurons from at least three mice per time point). (**C**) Cumulative probability distributions showing the same data as in (B). Injection of BrdU at E10 and E17 did not produce any detectable staining in the adult, thereby marking the beginning and the end, respectively, of the MEC neurogenesis window. (**D**) DCX expression in stellate and pyramidal neurons born on the same day at different dorsoventral positions along the MEC (>20,000 neurons from at least three mice per time point). BrdU was injected at E13, and only stellate and pyramidal cells labeled by BrdU were considered for the analysis. The fraction of DCX$^-$ BrdU-labeled cells was determined at three time points during network maturation (P11, P14, and P17; color-coded).

were not affected by the recovery from MEC silencing ($F_{7,32} < 0.82$, $P > 0.81$; fig. S7, B and C).

Maturation of stellate cells correlates with birth date

The silencing experiments suggest that maturation of stellate cells occurs independently of local excitatory activity and that it might instead rely on a signal intrinsic to these cells. A strong predictor of maturation may be the cells' birth date. Neurogenesis initiates a cascade of cell-autonomous transcriptional events that direct the differentiation of neurons in a stereotyped manner (*29*). If the timing of maturation in stellate cells was determined by neurogenesis, then we would expect cells to be topographically arranged according to birth date along the dorsoventral MEC axis, with the oldest neurons at the dorsal end and the youngest ventrally. To test this prediction, we injected 5-bromo-2′-deoxyuridine (BrdU) during gestation to quantify the proportion of local cells that underwent cell division at the time of injection and then mapped their distribution in the adult (Fig. 4A and fig. S8A).

Our analysis revealed that, although entorhinal pyramidal cells and PV interneurons were distributed randomly with respect to birth date (two-way ANOVA, Segment × Injection Day: $F_{7,36} = 0.23$, $P = 0.98$ for pyramidal cells and $F_{7,36} = 0.15$, $P = 0.87$ for PV$^+$ interneurons; Fig. 4, B and C, and fig. S8B, respectively), stellate cells exhibited an orderly birth date–dependent distribution along the dorsoventral MEC axis. Early-born stellate cells were prevailingly (but not exclusively) located at the dorsal MEC pole, whereas later-born cells were found at progressively more ventral positions (two-way ANOVA with Segment and Injection Day as factors: $F_{7,36} = 105.32$, $P < 0.0001$; for each segment: $F_{5,24} > 4.301$, $P < 0.006$; Fig. 4, B and C, and fig. S8C).

To verify the association between the topographies of neurogenesis and maturation, we further analyzed DCX expression in "isochronic cells"—cells that were born on the same day (*29*). If maturation is entirely dependent on neurogenesis, then the fraction of DCX$^-$ cells should be at comparable levels among isochronic neurons, independent of their dorsoventral location. We found that, among embryonic day 13 (E13)–born stellate cells, there was no effect of dorsoventral location on the fraction of DCX$^-$ cells (two-way ANOVA with Segment for each of the three time points: $F < 0.837$ and $P > 0.3$; Fig. 4D, left). In contrast, among E13-born pyramidal cells, the fraction of DCX$^-$ cells remained correlated with anatomical position (two-way ANOVA, only Segment considered: $F > 29.8$ and $P > 0.0001$; Fig. 4D, right). This experiment confirms that maturation of stellate cells, but not pyramidal cells, is intrinsically correlated with birth date.

Stellate cells drive stagewise network maturation

Because the silencing experiments point to local excitatory activity in MEC-L2 as the main drive for pyramidal cell maturation, we next asked whether stellate cells might be the source. To achieve cell type–specific silencing, we exploited the staggered neurogenesis of stellate and pyramidal cells (fig. S8D). Because nearly all dorsal MEC cells from early isochronic cohorts are stellate cells, whereas those from late cohorts are predominantly pyramidal cells, it should be possible to distinguish between them by labeling cells either at the beginning or at the end of the neurogenesis window for dorsal MEC.

To gain genetic access to cells born within specific time windows during neurogenesis, we developed a method based on in utero injection of an insertion-deficient, recombinant adeno-associated virus (AAV) into the lateral ventricle

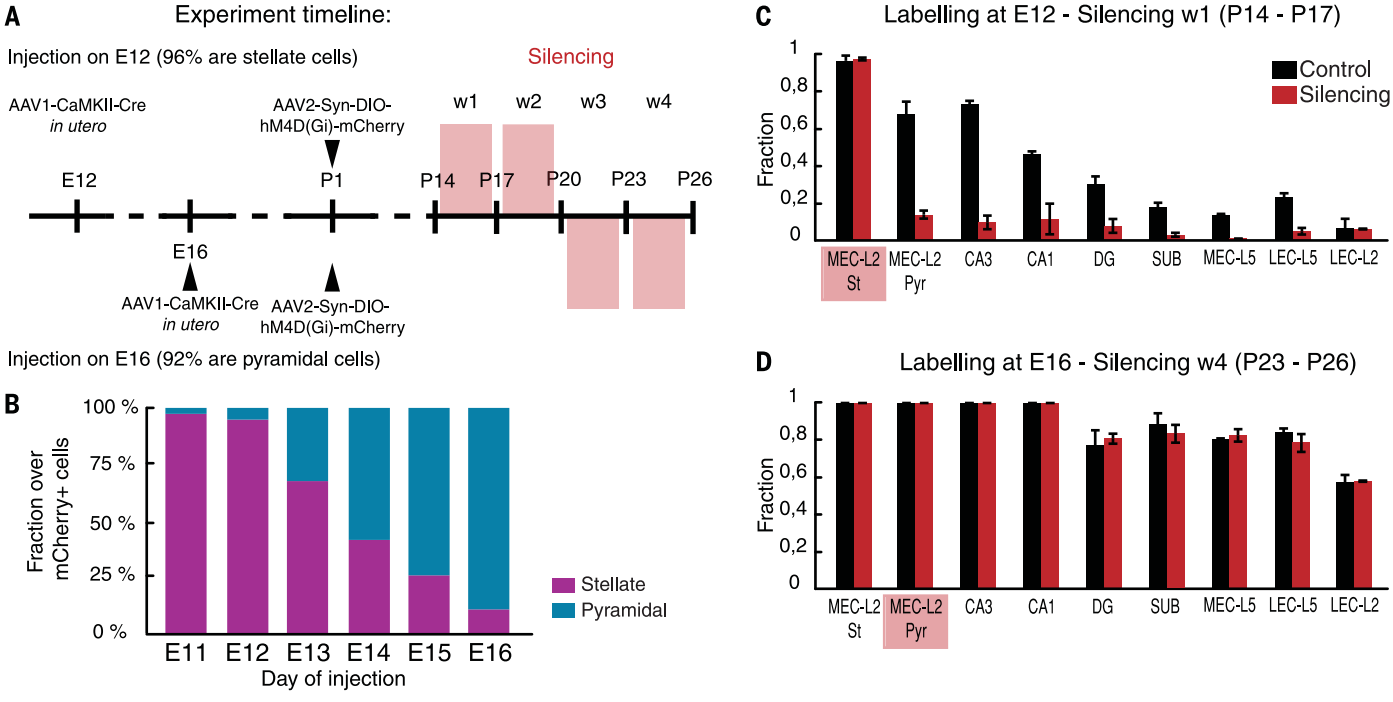

Fig. 5. Excitatory activity from stellate cells drives network maturation. (**A**) Schematic illustrating the experiment. (**B**) Molecular identity of infected neurons as a function of the embryonic day of viral injection. *Y* axis, fraction of mCherry$^+$ cells that coexpress a marker for stellate cells (reelin) or pyramidal cells (calbindin) (>54,000 neurons from at least three animals per time point). (**C**) Fraction of DCX$^-$ cells in different regions of the entorhinal-hippocampal network upon silencing of isochronic cohorts dominated by stellate cells in MEC-L2 (E12-born; means ± SD). The fraction of neurons showing down-regulated DCX expression after silencing is different from control animals in all cell types and areas, with the exception of MEC-L2 St and LEC-L2. The lack of effect on LEC-L2 is likely due to the immaturity of this local network at P17 (note low value in control animals). All comparisons with Student's *t* test were significant ($t > 7.44$ and $P < 0.01$), with the exception of LEC-L2 ($t = 0.36$ and $P = 0.70$). Analyses were conducted in the dorsal entorhinal cortex and hippocampus (>27,000 neurons from at least three mice per experimental group). Three categorically different classes of treatment were pooled to form the control group, as in Fig. 2. (**D**) Fraction of DCX$^-$ cells upon silencing of isochronic cohorts dominated by pyramidal neurons (E16-born; means ± SD). DCX expression in silenced animals is indistinguishable from that of controls ($t < 1.03$ and $P > 0.34$). Similar effects were obtained with other silencing windows (figs. S11 and S12). Analysis was conducted with similar control groups and a similar number of neurons and animals as in (B).

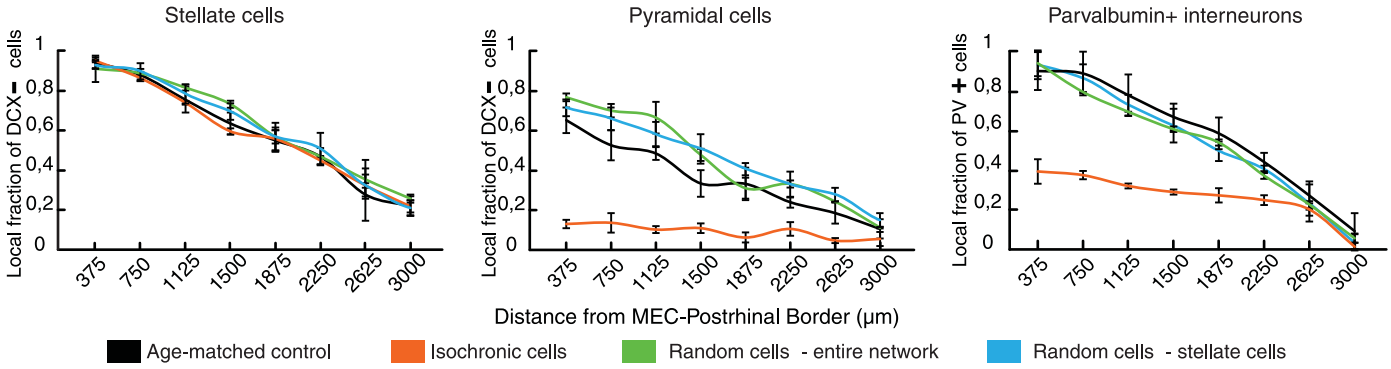

Fig. 6. Isochronic cohorts of neurons act synergistically to drive MEC-L2 maturation. Quantitative analysis of network maturation based on DCX expression along the dorsoventral axis of MEC-L2. DCX$^-$ pyramidal cells and PV$^+$ interneurons disappear when an isochronic population of E12-born neurons is silenced (orange), but not when the ligand targets a comparable fraction of randomly labeled L2 cells (green, "Random cells – entire network": 20% of MEC-L2 excitatory neurons labeled) or stellate cells (blue, "Random cells – stellate cells": 20% of MEC-L2 stellate cells labeled) (>45,000 neurons from three animals per group). Three categorically different classes of treatment were pooled to form the control group, as in Fig. 2.

of the developing brain (fig. S9A). The localization of the virus to the ventricle allowed for selective targeting of the viral construct to postmitotic cells that had not yet, at the time of infection, migrated out of the ventricular zone where they were born (fig. S9A). Using a double viral-BrdU approach, we found that the method was specific in targeting cells born on the day of the viral injection in MEC-L2, within a time window of 24 to 32 hours (fig. S9, B and D). The method was validated on sections from visual cortex, where, as expected, neurogenesis showed an inside-out progression, with E12 injections only labeling cells in the deepest layers and E16 injections targeting exclusively cells in superficial layers (fig. S9E) (*30*, *31*). In MEC, the topographical distribution and dorsoventral progression of neurogenesis were identical in BrdU and virally identified cohorts (fig. S9F).

Using the viral approach, we were able to test the hypothesis that activity in stellate but not pyramidal cells is necessary for driving maturation throughout the entorhinal-hippocampal circuit. We first injected a Cre virus (AAV1-CaMKII-Cre) into the lateral ventricle at either E12 or E16 to prime isochronic cohorts of cells to express the recombinase Cre. Then, at P1, we targeted the inhibitory DREADD hM4D(Gi) to primed cells by injecting the Cre-dependent virus in MEC-L2. Finally, during multiple time windows of postnatal maturation, we delivered CNO through osmotic minipumps, as in the previous experiments (Fig. 5A). Both cohorts of animals received CNO during a time window of 3 days (w1, P14 to P17; w2, P17 to P20; w3, P20 to P23; w4, P23 to P26). We silenced early-born neurons (E12-labeled) during early (w1 and w2) and late (w3) windows of maturation (fig. S11) and late-born neurons during early (w2) and late (w3 and w4) windows (fig. S12). As expected, in the most dorsal part of the MEC, the composition of the labeled cohort was dominated by stellate cells when the injection was performed at E12 (96% of infected cells colocalized with reelin; Fig. 5B and fig. S10A). In contrast, pyramidal cells predominated when the viral mix was injected at E16 (92% of infected cells colocalized with calbindin; Fig. 5B and fig. S10A). Thus, at the dorsal pole of the MEC, silencing of E12-born cells inactivated almost exclusively stellate cells, whereas silencing of E16-born cells inactivated almost only pyramidal cells. The two approaches labeled comparable fractions of neurons in the overall layer 2 network (Student's t test, $t = 0.72$ and $P = 0.98$; fig. S10B).

Inactivation during postnatal maturation revealed that stellate cell–specific silencing was sufficient to block maturation of pyramidal cells in MEC-L2 (two-way ANOVA with Group and Segment as factors; Group: $F_{1,32} = 27.01$, $P < 0.001$; Group × Segment: $F_{7,32} = 83.9$, $P < 0.0001$; fig. S11A). In a similar fashion, silencing stellate cells born at E12 prevented maturation of PV$^+$ interneurons (Group: $F_{1,32} = 15.92$, $P < 0.001$; Group × Segment: $F_{7,32} = 64.20$, $P < 0.0001$; fig. S11A). As expected from the global layer 2 interventions described earlier, the stellate cells themselves were not affected (Group: $F_{1,32} = 0.981$, $P = 0.78$; Group × Segment: $F_{7,32} = 2.30$, $P = 0.30$; fig. S11A).

In contrast, pyramidal cell–specific inactivation did not affect the expression of DCX in the pyramidal cells themselves (Group: $F_{1,32} = 1.59$, $P = 0.32$; Group × Segment: $F_{7,32} = 0.73$, $P = 0.51$; fig. S12C) or in stellate cells (two-way ANOVA, Group: $F_{1,32} = 1.72$, $P = 0.25$; Group × Segment: $F_{7,32} = 0.98$, $P = 0.23$; fig. S12C) and did not affect PV expression in interneurons (two-way ANOVA, Group: $F_{1,32} = 2.12$, $P = 0.08$; Group × Segment: $F_{7,32} = 1.04$, $P = 0.50$; fig. S12C). To test whether the ineffectiveness of pyramidal cell silencing was dependent on the timing of CNO delivery, we delivered CNO in adjacent time windows in a parallel set of experiments. No significant difference in DCX or PV expression could be detected between silenced and control animals when CNO was delivered in a time-unmatched fashion, with either stellate cell–specific silencing (Group: $F_{1,32} < 1.59$, $P > 0.70$; Group and Segment as factors; pyramidal cells or interneurons versus their controls: $F_{7,32} < 1.654$, $P > 0.54$; fig. S11, B and C) or selective silencing of pyramidal cells (Group: $F_{1,32} < 2.13$, $P > 0.15$; Group × Segment: $F_{7,32} < 2.124$, $P > 0.30$; fig. S12, A and B). Collectively, these experiments suggest that the activity in stellate but not pyramidal cells is necessary for the maturation of the local network in MEC-L2.

The localization of the instructive signal in MEC to stellate cells raises the question of whether activity from isochronic stellate cells might also be necessary for the sequential maturation across subdivisions of the transverse entorhinal-hippocampal circuit. Silencing isochronic stellate cells was sufficient to prevent the maturation-associated down-regulation of DCX in every area of the network (all comparisons with Student's t test were significant, $t > 7.44$ and $P < 0.01$, with the exception of LEC-L2, $t = 0.36$ and $P = 0.7$, where most cells were in an immature state under the control condition too; Fig. 5C and fig. S13A). Silencing stellate cells was also sufficient to decrease PV expression throughout the entorhinal-hippocampal loop (all comparisons were significant, $t > 6.23$ and $P < 0.01$, with the exception of LEC-L5 and LEC-L2, $t < 0.13$ and $P > 0.15$; fig. S13B, left). Synaptogenesis was similarly retarded (all comparisons were significant, $t > 4.71$ and $P < 0.01$; fig. S13B, right). In striking contrast, silencing isochronic pyramidal cells did not exert any effect on maturation of the transverse entorhinal-hippocampal circuit ($t < 1.03$ and $P > 0.34$; Fig. 5D and fig. S13, A and C). We also silenced stellate cells at later time points, between P20 and P23, after the maturation of their postsynaptic partners is complete. This had no effect on DCX expression at any stage of the entorhinal-hippocampal network ($t < 2.41$ and $P > 0.72$; fig. S13D), suggesting that the instructive role that stellate cells have on entorhinal-hippocampal circuit maturation is temporally limited. Together, the results identify stellate cells as the source of the activity-dependent instructive signal that drives the sequential maturation of the entorhinal-hippocampal network.

Isochronic cohorts of neurons act synergistically

By exploiting our method to genetically label isochronic cohorts of neurons, we were able to show

that silencing a small fraction of the MEC-L2 network is sufficient to interfere with maturation of the entorhinal-hippocampal circuit only if the silenced cohort predominantly consists of stellate cells (Fig. 5). At first glance, this observation is at odds with the observation in one of the earlier experiments that maturation requires silencing of more than 20% of the MEC-L2 cell population (fig. S6A). One major difference between the two sets of experiments is that cells infected in utero were not randomly drawn from the network but were born on the same day. If isochronic cells act synergistically during development, then silencing a small but isochronic fraction of the network might be sufficient to efficiently affect network maturation. To test this idea, we silenced the isochronic cohort of MEC-L2 excitatory cells born on E12 and compared the result with the silencing of a comparable fraction of neurons whose labeling was independent of neurogenesis (fig. S14A). The E12 isochronic cohort was primed for silencing in utero and then targeted with the Cre-dependent hM4D(Gi) receptor at P1 before delivery of CNO during postnatal development (fig. S14A, "Isochronic cells"). To label a comparable fraction of neurons randomly, we injected a mix of AAVs targeting hM4D(Gi) to excitatory cells postnatally at P1 to avoid any bias to birth date (fig. S14A, "Random cells"). The viruses were injected in proportions that allowed labeling of a sparse cohort of neurons, targeting a fraction of the L2 network ("Random cells – entire network") or a fraction of the stellate cells in MEC-L2 ("Random cells – stellate cells"), which was comparable to the isochronic cohort.

Partial silencing of MEC-L2 was sufficient to affect DCX expression in pyramidal cells and PV expression in interneurons only if the targeted neurons were born on the same day, but not if they were drawn randomly with respect to their birth date (Group × Segment: $F_{7,32} > 5.86, P < 0.001$; Group: $F_{1,32} > 83.90$, $P < 0.0001$ for isochronic cells; Group × Segment: $F_{7,32} < 1.78$, $P > 0.09$; Group: $F_{1,32} < 0.42$, $P > 0.87$ for random cells; Fig. 6). The effect of silencing was specific to the earliest window of circuit maturation (w1; Fig. 6); no effect was observed when CNO was delivered at later time points (Group × Segment: $F_{7,32} < 0.38$, $P > 0.62$; Group: $F_{1,32} < 3.22$, $P > 0.061$; w2 and w3; fig. S14C). In agreement with previous findings, stellate cells were not affected by silencing during any window of CNO delivery (Group: $F_{1,32} < 1.38$, $P > 0.211$; Group × Segment: $F_{7,32} < 0.61$, $P > 0.8$; Fig. 6 and fig. S14C). Together, these results indicate that isochronic cohorts of neurons in MEC-L2 exert a synergistic effect on microcircuit maturation.

Discussion

We have shown that the entorhinal-hippocampal network matures in a stereotyped and directional sequence that, with the exception of the DG, recapitulates the intrinsic excitatory connectivity of the transverse hippocampal circuit. At every level of the circuit, maturation and synaptogenesis rely on an excitatory activity-dependent instructive signal that originates in stellate cells of the MEC and spreads directionally throughout the circuit over the course of the first month of postnatal life. Stellate cells, being the first to mature, initiate maturation of the network by providing excitatory drive to their synaptic targets. These, in turn, subsequently exert a driving effect on areas further downstream, resulting in successive, stagewise maturation of the transverse entorhinal-hippocampal circuit. Maturation of stellate cells themselves is independent of local and incoming excitatory activity but correlates with birth date, pointing to cell-autonomous molecular, genetic, or epigenetic pathways, set up before birth, as potential sources of stellate cell–initiated maturation in the entorhinal-hippocampal circuit.

In line with the role that sensory-driven activity exerts in the primary sensory cortices, stellate cells might influence computation in the entorhinal-hippocampal network by orchestrating the refinement of connectivity within MEC and hippocampus, as well as between these structures. By driving structural maturation of the interneuron network and of the back projections from the hippocampus, stellate cells might serve as a developmental teaching layer to ensure strong coupling among cells that exhibit correlated neural activity in stimulus space (*32*). This may be crucial for the development of attractor network topologies thought to underlie the formation of grid patterns (*10*, *32*–*36*).

The progression of neurogenesis and maturation along the dorsoventral MEC axis may account for the topographic and modular organization of grid scale in grid cells along this axis. Moreover, because of the quantal nature of proliferation in neural progenitor cells (*37*), neurogenesis may contribute to discretization of grid cells into modules (*38*). The production of consecutive generations of "daughter cells" during neurogenesis may parcel stellate cells into cohorts that each are composed of neurons born on the same day (isochronic cells). Such waves of simultaneously born stellate cells may give rise to parallel networks with unique features, set up in ways that mirror the formation of parallel microcircuits of selectively interconnected neurons in the hippocampal trisynaptic loop (*26*, *39*). These subnetworks born at different times might correspond to the modules of grid cells, which have a similar anatomical distribution to the cohorts presented here (*38*).

The nature of the instructive signal spreading through the network and driving local circuit maturation remains to be determined. Specific spatial or temporal patterns of depolarization in the network might be required to elicit postsynaptic responses leading to synaptogenesis and maturation. One candidate activity pattern is the orchestrated change of calcium concentrations across populations of neurons defined as "calcium waves," which has been implicated in the establishment of topography in sensory areas (*40*, *41*). In the entorhinal-hippocampal circuit, isochronic neurons may exhibit similarly synchronized activity. Such activity may pattern network maturation stage by stage across the circuit (*42*). Isochronic neurons might exert a synergistic effect on maturation because of their tight temporal coupling during waves.

Our data show that stellate cells are at the top of the developmental hierarchy that instructs the linear sequence of maturation of the entorhinal-hippocampal circuit. Peripheral sensory organs have long been studied as the source of instructive signals driving the early development of the forebrain. For example, the olfactory organ instructs the central nervous system to reach its mature states (*43*–*45*), and, in a similar fashion, thalamocortical axons are involved in cortical regionalization and the refinement of dendritic arborization and connectivity in the visual, somatosensory, and auditory systems (*46*, *47*). Although activity from sensory organs provides a clear directionality to the maturation of cortical columns in sensory areas, we show here that, in the entorhinal-hippocampal circuit, it is the activity from stellate cells that drives the maturation of the entire circuit. Our data identify a network where such instructive excitatory activity does not originate from sensory neurons but is provided by a subpopulation of neurons that functions as an "autonomous" intrinsic driver in a neurogenesis-dependent manner. The presence of a few of these intrinsic drivers in the brain during development might be particularly influential for the coordinated maturation of networks that are positioned at a great synaptic distance from sensory signals and extend across multiple areas in the associative cortices, thereby shaping network topologies supporting higher cognitive function.

Materials and methods

All experiments were performed in accordance with the Norwegian Animal Welfare Act and the European Convention for the Protection of Vertebrate Animals used for Experimental and Other Scientific Purposes, Permit numbers 6021, 6008, and 7163. C57/Bl6 mice were housed in social groups of 2-6 individuals per cage under a 12h light/12h darkness schedule, in a temperature- and humidity-controlled vivarium. Food and water were provided ad libitum.

Viral injections

For all surgeries, on the day of the injection, anesthesia was induced by placing the subjects in a plexiglass chamber filled with isoflurane vapor (5% isoflurane in medical air, flow of 1 liters/minute). Surgery was performed on a heated surgery table (38°C), air flow was kept at 1 liters/minute with 1.5–3% isoflurane as determined from physiological monitoring of vital signs (breathing and heartbeat). Analgesics were provided immediately before the surgery (Rymadil, Pfizer, 5 mg/kg). After each procedure, subjects were allowed to recover in a heated chamber (33°C, 30–90 min) until they regained complete mobility and alertness.

Viral injections at P1

Newborn pups were subjected to viral injection 1 day after birth (P1). Pre-heated ultrasound gel (39°C, Aquasonic 100, Parker) was generously applied on the pup's head in order to create a large medium for the transmission of ultrasound waves.

Real-time ultrasound imaging (Vevo 1100 System, Fujifilm Visualsonics) allowed for targeted delivery of the viral mixture to specific areas. For imaging, the ultrasound probe (MS-550S) was lowered to be in close contact with the gel to allow visualization of the targeted structures, and was kept in place for the whole duration of the procedure via the VEVO injection mount (VEVO Imaging Station. Imaging in B-Mode, frequency: 40 MHz; power: 100%; gain: 29 Db; dynamic range: 60 Db). Target regions were identified by structural landmarks: the hippocampus was identified by the cytoarchitecture of CA3 and the appearance of the lateral ventricle (target area for injection was comparable to a coronal section at -1.46 mm from bregma in the adult animal (*48*)); the MEC and LEC were identified by the appearance of the aqueduct of Sylvius and the lateral sinus (target area for injection was comparable to a coronal section at -4.72 mm from bregma in the adult animal (*48*)).

A viral mixture (250 ± 50 nl per injection) was injected in the target regions via beveled glass micropipettes (Origio, custom made. Outer tip opening: 200 μm. Inner tip opening: 50 μm) with a pressure-pulse system (Visualsonics, 5 pulses, 50 nl per pulse). The anatomical specificity of the infection was verified by imaging serial sections of the infected hemispheres after experiment completion.

Virus injection in the embryo

Pregnant females were subjected to the viral injection on a specific day of gestation, from E10 to E17. To achieve precise monitoring of gestation, a mating trio (one male and two females) was allowed to interact for a limited period of time (24 hours), after which the male was removed from the cage to prevent further mating. E1 was defined as the day on which the male was removed (vaginal plug could be observed in most of the cases). A longitudinal incision was performed on the shaved skin and peritoneum of the isoflurane anaesthetized female to reach the uterine horns. The abdominal cavity was kept irrigated with warm saline solution (0.9% NaCl, 39°C) for the entire procedure. Single embryos were transferred one-by-one to a custom made, sterile surgical chamber to allow for viral injection. Pre-heated ultrasound gel (39°C, Aquasonic 100, Parker) was generously applied to the embryos. Real-time ultrasound imaging (parameters as above) allowed for targeted delivery of the viral mixture to the lateral ventricle of the developing brain. The viral solution (containing AAV1-CaMKII-Cre; 150–350 nl per injection) was applied as previously described (UPenn Vector Core, University of Pennsylvania, Perelman School of Medicine). After injection, the ultrasound gel was removed with sterile gauze and the embryo placed back into the abdominal cavity. This procedure was repeated for all the other embryos in the litter. After injection of the last embryo, two independent sets of stitches were applied to the peritoneum and abdominal skin. The total length of the procedure was limited to less than 90 min to avoid unnecessary stress to the mother and the embryos. 80% of the injected embryos survived injection and delivery, and could be utilized for further studies.

Pharmacogenetic silencing

On P11 or P14, a longitudinal incision was performed on the shaved skin of the isoflurane anaesthetized pup's back in order to allow for the insertion of a minipump subcutaneously. Warm saline solution (0.9% NaCl, 39°C) was injected subcutaneously in the area of the incision at multiple times during the minipump implant. The osmotic minipump (Alzet, 1007D: flow of 0.5 μl per hour for up to 7 days) filled with 100 μl of CNO solution (1 mg/ml in saline solution, Sigma) was then placed through the incision to rest comfortably on the mouse's back. No impairment of normal behavior as a result of discomfort from the implant could be observed in the days following the procedure. CNO delivery was protracted over the course of several days during maturation, with a steady flow of 0.5 μl per hour according to the manufacturer's specification (Alzet). In a subset of P14-implanted animals (14 subjects), the minipump was surgically removed at P20 through a second incision. Seven subjects were perfused after 3 days of recovery (P23), while another 7 were perfused after 6 days of recovery (P26) and processed for further analysis.

REFERENCES AND NOTES

1. W. Penfield, W. P. E. Boldrey, Somatic motor and sensory representation in the cerebral cortex of man as studied by electrical stimulation. *Brain* **60**, 389–443 (1937). doi: 10.1093/brain/60.4.389
2. V. B. Mountcastle, Modality and topographic properties of single neurons of cat's somatic sensory cortex. *J. Neurophysiol.* **20**, 408–434 (1957). pmid: 13439410
3. D. H. Hubel, T. N. Wiesel, Receptive fields, binocular interaction and functional architecture in the cat's visual cortex. *J. Physiol.* **160**, 106–154 (1962). doi: 10.1113/jphysiol.1962.sp006837
4. A. D. Huberman, M. B. Feller, B. Chapman, Mechanisms underlying development of visual maps and receptive fields. *Annu. Rev. Neurosci.* **31**, 479–509 (2008). doi: 10.1146/annurev.neuro.31.060407.125533; pmid: 18558864
5. T. N. Wiesel, D. H. Hubel, Effects of visual deprivation on morphology and physiology of cells in the cat's lateral geniculate body. *J. Neurophysiol.* **26**, 978–993 (1963). pmid: 14084170
6. D. H. Hubel, T. N. Wiesel, Receptive fields of cells in striate cortex of very young, visually inexperienced kittens. *J. Neurophysiol.* **26**, 994–1002 (1963). pmid: 14084171
7. L. Galli, L. Maffei, Spontaneous impulse activity of rat retinal ganglion cells in prenatal life. *Science* **242**, 90–91 (1988). doi: 10.1126/science.3175637; pmid: 3175637
8. L. C. Katz, C. J. Shatz, Synaptic activity and the construction of cortical circuits. *Science* **274**, 1133–1138 (1996). doi: 10.1126/science.274.5290.1133; pmid: 8895456
9. D. C. Rowland, Y. Roudi, M.-B. Moser, E. I. Moser, Ten years of grid cells. *Annu. Rev. Neurosci.* **39**, 19–40 (2016). doi: 10.1146/annurev-neuro-070815-013824; pmid: 27023731
10. E. I. Moser *et al*., Grid cells and cortical representation. *Nat. Rev. Neurosci.* **15**, 466–481 (2014). doi: 10.1038/nrn3766; pmid: 24917300
11. S. R. y Cajal, Estructura del asta de Ammon y fascia dentata. *Ann. Soc. Esp. Hist. Nat.* **22**, 53–114 (1893).
12. R. L. de Nó, Studies on the structure of the cerebral cortex. II. Continuation of the study of the ammonic system. *J. Psychol. Neurol.* **46**, 113–177 (1934).
13. M. P. Witter, E. I. Moser, Spatial representation and the architecture of the entorhinal cortex. *Trends Neurosci.* **29**, 671–678 (2006). doi: 10.1016/j.tins.2006.10.003; pmid: 17069897
14. N. L. M. Cappaert, N. M. Van Strien, M. P. Witter, Hippocampal formation, in *The Rat Nervous System* (Academic Press, 2015), pp. 511–573.
15. R. F. Langston *et al*., Development of the spatial representation system in the rat. *Science* **328**, 1576–1580 (2010). doi: 10.1126/science.1188210; pmid: 20558721
16. T. J. Wills, F. Cacucci, N. Burgess, J. O'Keefe, Development of the hippocampal cognitive map in preweanling rats. *Science* **328**, 1573–1576 (2010). doi: 10.1126/science.1188224; pmid: 20558720
17. T. L. Bjerknes, E. I. Moser, M.-B. Moser, Representation of geometric borders in the developing rat. *Neuron* **82**, 71–78 (2014). doi: 10.1016/j.neuron.2014.02.014; pmid: 24613417
18. T. L. Bjerknes, R. F. Langston, I. U. Kruge, E. I. Moser, M.-B. Moser, Coherence among head direction cells before eye opening in rat pups. *Curr. Biol.* **25**, 103–108 (2015). doi: 10.1016/j.cub.2014.11.009; pmid: 25466682
19. L. Muessig, J. Hauser, T. J. Wills, F. Cacucci, A developmental switch in place cell accuracy coincides with grid cell maturation. *Neuron* **86**, 1167–1173 (2015). doi: 10.1016/j.neuron.2015.05.011; pmid: 26050036
20. J. G. Gleeson, P. T. Lin, L. A. Flanagan, C. A. Walsh, Doublecortin is a microtubule-associated protein and is expressed widely by migrating neurons. *Neuron* **23**, 257–271 (1999). doi: 10.1016/S0896-6273(00)80778-3; pmid: 10399933
21. J. Nacher, C. Crespo, B. S. McEwen, Doublecortin expression in the adult rat telencephalon. *Eur. J. Neurosci.* **14**, 629–644 (2001). doi: 10.1046/j.0953-816x.2001.01683.x; pmid: 11556888
22. H. van Praag, G. Kempermann, F. H. Gage, Running increases cell proliferation and neurogenesis in the adult mouse dentate gyrus. *Nat. Neurosci.* **2**, 266–270 (1999). doi: 10.1038/6368; pmid: 10195220
23. D. Doischer *et al*., Postnatal differentiation of basket cells from slow to fast signaling devices. *J. Neurosci.* **28**, 12956–12968 (2008). doi: 10.1523/JNEUROSCI.2890-08.2008; pmid: 19036989
24. S. Dieck *et al*., Bassoon, a novel zinc-finger CAG/glutamine-repeat protein selectively localized at the active zone of presynaptic nerve terminals. *J. Cell Biol.* **142**, 499–509 (1998). doi: 10.1083/jcb.142.2.499; pmid: 9679147
25. J. B. Angevine Jr., Time of neuron origin in the hippocampal region: An autoradiographic study in the mouse. *Exp. Neurol. Suppl.* **2**, 1–70 (1965). pmid: 5838955.
26. Y. Deguchi, F. Donato, I. Galimberti, E. Cabuy, P. Caroni, Temporally matched subpopulations of selectively interconnected principal neurons in the hippocampus. *Nat. Neurosci.* **14**, 495–504 (2011). doi: 10.1038/nn.2768; pmid: 21358645
27. C. Miao *et al*., Hippocampal remapping after partial inactivation of the medial entorhinal cortex. *Neuron* **88**, 590–603 (2015). doi: 10.1016/j.neuron.2015.09.051; pmid: 26539894
28. S. Ray, M. Brecht, Structural development and dorsoventral maturation of the medial entorhinal cortex. *Elife* **5**, e13343 (2016). doi: 10.7554/eLife.13343; pmid: 27036175
29. L. Telley *et al*., Sequential transcriptional waves direct the differentiation of newborn neurons in the mouse neocortex. *Science* **351**, 1443–1446 (2016). doi: 10.1126/science.aad8361; pmid: 26940868
30. J. B. Angevine Jr., R. L. Sidman, Autoradiographic study of cell migration during histogenesis of cerebral cortex in the mouse. *Nature* **192**, 766–768 (1961). doi: 10.1038/192766b0; pmid: 17533671
31. P. Rakic, Neurons in rhesus monkey visual cortex: Systematic relation between time of origin and eventual disposition. *Science* **183**, 425–427 (1974). doi: 10.1126/science.183.4123.425; pmid: 4203022
32. B. L. McNaughton, F. P. Battaglia, O. Jensen, E. I. Moser, M.-B. Moser, Path integration and the neural basis of the 'cognitive map'. *Nat. Rev. Neurosci.* **7**, 663–678 (2006). doi: 10.1038/nrn1932; pmid: 16858394
33. Y. Burak, I. R. Fiete, Accurate path integration in continuous attractor network models of grid cells. *PLOS Comput. Biol.* **5**, e1000291 (2009). doi: 10.1371/journal.pcbi.1000291; pmid: 19229307
34. J. J. Couey *et al*., Recurrent inhibitory circuitry as a mechanism for grid formation. *Nat. Neurosci.* **16**, 318–324 (2013). doi: 10.1038/nn.3310; pmid: 23334580
35. M. C. Fuhs, D. S. Touretzky, A spin glass model of path integration in rat medial entorhinal cortex. *J. Neurosci.* **26**, 4266–4276 (2006). doi: 10.1523/JNEUROSCI.4353-05.2006; pmid: 16624947
36. T. Bonnevie *et al*., Grid cells require excitatory drive from the hippocampus. *Nat. Neurosci.* **16**, 309–317 (2013). doi: 10.1038/nn.3311; pmid: 23334581

37. P. Gao *et al*., Deterministic progenitor behavior and unitary production of neurons in the neocortex. *Cell* **159**, 775–788 (2014). doi: 10.1016/j.cell.2014.10.027; pmid: 25417155
38. H. Stensola *et al*., The entorhinal grid map is discretized. *Nature* **492**, 72–78 (2012). doi: 10.1038/nature11649; pmid: 23222610
39. S. Druckmann *et al*., Structured synaptic connectivity between hippocampal regions. *Neuron* **81**, 629–640 (2014). doi: 10.1016/j.neuron.2013.11.026; pmid: 24412418
40. M. Meister, R. O. Wong, D. A. Baylor, C. J. Shatz, Synchronous bursts of action potentials in ganglion cells of the developing mammalian retina. *Science* **252**, 939–943 (1991). doi: 10.1126/science.2035024; pmid: 2035024
41. C. S. Goodman, C. J. Shatz, Developmental mechanisms that generate precise patterns of neuronal connectivity. *Cell* **72**, 77–98 (1993). doi: 10.1016/S0092-8674(05)80030-3; pmid: 8428376
42. X. Leinekugel *et al*., Correlated bursts of activity in the neonatal hippocampus in vivo. *Science* **296**, 2049–2052 (2002). doi: 10.1126/science.1071111; pmid: 12065842
43. H. S. Burr, The effects of the removal of the nasal pits in Amblystoma embryos. *J. Exp. Zool.* **20**, 27–57 (1916). doi: 10.1002/jez.1400200202
44. R. Levi-Montalcini, The development to the acoustico-vestibular centers in the chick embryo in the absence of the afferent root fibers and of descending fiber tracts. *J. Comp. Neurol.* **91**, 209–241 (1949). doi: 10.1002/cne.900910204; pmid: 15408222
45. L. Dryer, P. P. Graziadei, Influence of the olfactory organ on brain development. *Perspect. Dev. Neurobiol.* **2**, 163–174 (1994). pmid: 7728500
46. P. Rakic, Specification of cerebral cortical areas. *Science* **241**, 170–176 (1988). doi: 10.1126/science.3291116
47. G. López-Bendito, Z. Molnár, Thalamocortical development: How are we going to get there? *Nat. Rev. Neurosci.* **4**, 276–289 (2003). doi: 10.1038/nrn1075; pmid: 12671644
48. G. Paxinos, K. Franklin, *Paxinos and Franklin's the Mouse Brain in Stereotaxic Coordinates* (Academic Press, ed. 4, 2012).
49. P. Andersen, T. V. Bliss, K. K. Skrede, Lamellar organization of hippocampal pathways. *Exp. Brain Res.* **13**, 222–238 (1971). doi: 10.1007/BF00234087; pmid: 5570425
50. O. Steward, Topographic organization of the projections from the entorhinal area to the hippocampal formation of the rat. *J. Comp. Neurol.* **167**, 285–314 (1976). doi: 10.1002/cne.901670303; pmid: 1270625
51. L. W. Swanson, W. M. Cowan, An autoradiographic study of the organization of the efferent connections of the hippocampal formation in the rat. *J. Comp. Neurol.* **172**, 49–84 (1977). doi: 10.1002/cne.901720104; pmid: 65364
52. M. F. Yeckel, T. W. Berger, Feedforward excitation of the hippocampus by afferents from the entorhinal cortex: Redefinition of the role of the trisynaptic pathway. *Proc. Natl. Acad. Sci. U.S.A.* **87**, 5832–5836 (1990). doi: 10.1073/pnas.87.15.5832; pmid: 2377621
53. A. Hjorth-Simonsen, Hippocampal efferents to the ipsilateral entorhinal area: An experimental study in the rat. *J. Comp. Neurol.* **142**, 417–437 (1971). doi: 10.1002/cne.901420403; pmid: 4106861

ACKNOWLEDGMENTS

We thank A. M. Amundsgård, A. Burøy, V. Frolov, K. Haugen, E. Kråkvik, B. B. Løfaldli, and H. Waade for technical assistance; P. Caroni, S. Arber, and P. Capelli for training on in utero injections; C. Kentros and R. Raveendran for viral reagents; and M. Witter for discussion. This work was supported by two Advanced Investigator Grants from the European Research Council ("GRIDCODE" grant agreement no. 338865 and "ENSEMBLE" grant agreement no. 268598), the Kavli Foundation, the Egil and Pauline Braathen and Fred Kavli Centre for Cortical Microcircuits, the Louis-Jeantet Prize for Medicine, the Centre of Excellence Scheme and the National Infrastructure Scheme of the Research Council of Norway (Centre for Neural Computation grant agreement no. 223262, "NORBRAIN1" grant agreement no. 197467), and the European Molecular Biology Organization long-term fellowship (ALTF 246-2013). F.D., M.-B.M., and E.I.M. designed the experiments and analyses. F.D. and R.I.J. performed the experiments. F.D. performed the analyses. F.D. and E.I.M. wrote the paper with input from all authors.

SUPPLEMENTARY MATERIALS

www.sciencemag.org/content/355/6330/eaai8178/suppl/DC1
Materials and Methods
Figs. S1 to S14
References (*54*–*56*)

18 August 2016; accepted 23 January 2017
10.1126/science.aai8178

Stellate cells drive maturation of the entorhinal-hippocampal circuit

Flavio Donato, R. Irene Jacobsen, May-Britt Moser and Edvard I. Moser

Science **355** (6330), eaai8178.
DOI: 10.1126/science.aai8178originally published online February 2, 2017

The lights go on in order

Grid cells and place cells in the brain function as part of a circuit that helps us figure out where we are in our physical world. Donato *et al.* examined how that circuit develops in the brains of mice. Expression patterns of doublecortin and parvalbumin revealed that neurons in the circuit mature in the order in which information flows. Maturation of each piece of the circuit depends on excitatory neuronal activity from the preceding portion. Stellate cells, in contrast, follow an endogenous maturation program. The stellate cells are responsible for initiating the circuit's developmental progression.

Science, this issue p. eaai8178